ARCHIVES OF MECHANICS
Arch. Mech. **74** (1), 13–37, 2022, DOI: 10.24423/aom.3929

The partial slip contact problem for a monoclinic coated half plane

İ. ÇÖMEZ[1)], Y. ALINIA[2)], M. A. GÜLER[3)]

[1)] *Department of Civil Engineering, Karadeniz Technical University, Trabzon, Turkey*

[2)] *Department of Mechanical Engineering, Hakim Sabzevari University, Sabzevar, Iran, e-mail: y.alinia@hsu.ac.ir*

[3)] *College of Engineering and Technology, American University of the Middle East, Kuwait*

In this study, the partial slip contact problem for a monoclinic coated half plane indented by a rigid cylindrical punch is considered. The main objective of current study is to illustrate the effects of material anisotropy on the surface stresses, the contact width and the stick/slip region of the partial slip contact. Using the Fourier integral transform and boundary conditions of the problem, the singular integral equation of the system is obtained. Numerical results of the problem are provided for typical fibrous composites applying the Gauss-Chebyshev discretization method. Sensitivity analysis of the surface stresses is performed for both the material and geometric parameters. The results indicate that the coating fiber angle can significantly alter the distribution of contact tractions. As the fiber angle ranges from $\theta = 0^\circ$ to $\theta = 90^\circ$, the contact half-length increases up to 20% whereas the stick zone half-length varies significantly.

Key words: partial slip, monoclinic materials, fiber angle, stick/slip transition.

1. Introduction

One of the failure mechanisms that appears due to the small amount of relative displacement in the contacting components due to the repeated reversal of the tangential force in the slip region is the fretting wear. It is usually seen in aviation and automotive industry components such as the dove tail region of blade and disc arrangements in gas turbines (Ciavarella and Demelio [1], Rajasekaran and Nowell [2]), bolted joints (Juoksukangas *et al.* [3], Jiménez-Peña *et al.* [4]), connecting rods (Chao [5]), bearings in wind turbine rotor shafts (Rauert *et al.* [6]), spline couplings (Ding [7], Houghton [8]), suspension components (Buciumeanu [9]) etc. Mohrbacher *et al.* [10] defined three different modes of fretting, namely: mode I due to tangential loading, mode II due to normal loading and mode III due to torsional loading. According to Zhou and Vincent [11], there are three regimes in a fretting contact

depending on the sliding conditions such as the partial slip regime, the mixed regime and the gross slip regime. It is also reported that partial slip regime is responsible for crack nucleation and crack formation whereas gross slip regime is responsible for wear (Vincent *et al.* [12]). Therefore, understanding the partial slip contact mechanism is important since it may lead to fretting fatigue failure.

There is a wide range of study conducted in the fretting fatigue related studies. However, we limit our concentration to the studies related to the partial slip contact. In this sense, crack initiation and propagation caused by a partial slip regime was analyzed experimentally by Kuno *et al.* [13]. The fretting wear problem for an elastic medium under gross slip and partial slip conditions was studied by Gallego and Neilias [14]. Goryacheva [15] studied wear due to partial slip and concluded that crack nucleation can occur at the edge of the contact for a small number of cycles whereas it takes a large number of cycles to nucleate a crack at the stick/slip boundary. Andresen *et al.* [16] presented a method to solve a partial slip contact problem for a half-plane where there exist a bulk tension parallel to the interface and another one where there is asymmetry of the contact through introduction of a moment (Andresen *et al.* [17]). The method can determine the coordinates of the stick zone wherever it may be in the contact zone.

Herein, we give a short review of the contact mechanics studies related to anisotropic materials. There have been several methods utilized to solve the contact problems involving anisotropic materais such as complex variable formulation (Galin [18]), the conjugate gradient method (Bagault *et al.* [19]), Eshelby–Stroh formalism (Fan and Keer, [20]), Green–Lindsay thermo-elasticity (Brock and Georgiadis [21]), discrete convolution and the Fourier transform method (Hayashi *et al.* [22]), the boundary element method (Rodríguez-Tembleque *et al.* [23], Rodríguez-Tembleque *et al.* [24]). However, there are few studies available in the literature about a partial slip contact of anisotropic materials. Alinia and Guler [25] solved a fully coupled partial slip contact problem between an orthotropic medium and flat/ parabolic stamp profiles. Wang and coworkers [26, 27] solved the partial slip contact problems for a piezoelectric half-plane indented by a flat punch (Su *et al.* [26]) and a cylindrical punch (Su *et al.* [27]). Later, they extended the problem for the piezoelectric layered half-plane under a conducting punch (Su *et al.* [28]). In this study, we extend the partial slip contact problem solved by Comez *et al.* [29] for a monoclinic half plane to the coated half-plane problem for a monoclinic layer. To the best of authors' knowledge, this problem has not been solved in the open literature. The current study emphasizes the effect of several parameters such as the orientation of the material principal directions, the coefficient of friction, the material property and the substrate stiffness on the stress field.

2. Formulation of the problem

The plane partial slip contact problem of a monoclinic layer bonded to an isotropic half plane is depicted in Fig 1. The layer is indented by a rigid cylindrical punch with a radius of R that transmits the normal load P. The contact region $-a \le x \le a$ is assumed to consist of two regions, that is, a central stick zone $|x| \le b$ and an outer slip region $b \le |x| \le a$ with a finite friction coefficient, η.

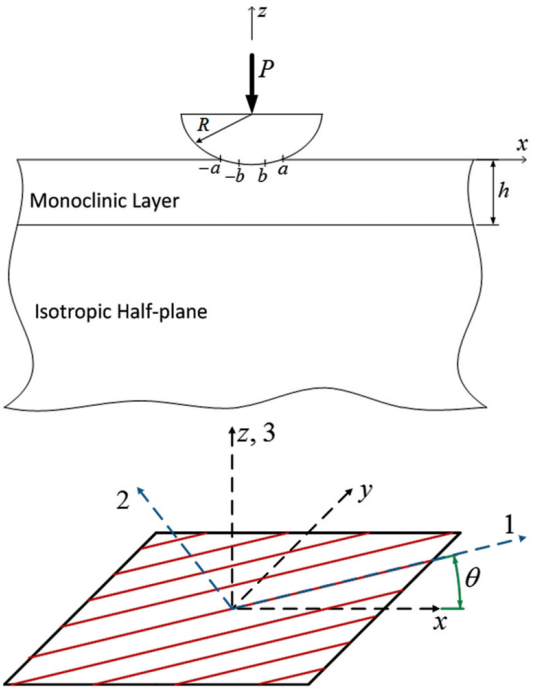

FIG. 1. Geometry of the contact problem and the definition of the fiber angle orientation.

Using the elasticity theory and the integral transform technique, the displacement and the stress components for the homogeneous monoclinic layer can be obtained as follows [30]:

$$u_1(x,z) = \frac{1}{2\pi} \int_{-\infty}^{\infty} \Big[\sum_{j=1}^{6} A_j \, e^{n_j \xi z}\Big] e^{-I\xi x} \, d\xi, \tag{2.1a}$$

$$v_1(x,z) = \frac{1}{2\pi} \int_{-\infty}^{\infty} \Big[\sum_{j=1}^{6} I k_j A_j \, e^{n_j \xi z}\Big] e^{-I\xi x} \, d\xi, \tag{2.1b}$$

$$w_1(x,z) = \frac{1}{2\pi}\int\limits_{-\infty}^{\infty}\Big[\sum_{j=1}^{6} Im_jA_j\, e^{n_j\xi z}\Big]e^{-I\xi x}\,d\xi, \tag{2.1c}$$

$$\sigma_{x1}(x,z) = \frac{1}{2\pi}\int\limits_{-\infty}^{\infty}\Big[-I\xi\sum_{j=1}^{6} A_j(\bar{C}_{11}+\bar{C}_{16}m_j-\bar{C}_{13}k_jn_j)\, e^{n_j\xi z}\Big]e^{-I\xi x}\,d\xi, \tag{2.1d}$$

$$\sigma_{y1}(x,z) = \frac{1}{2\pi}\int\limits_{-\infty}^{\infty}\Big[-I\xi\sum_{j=1}^{6} A_j(\bar{C}_{12}+\bar{C}_{26}m_j-\bar{C}_{23}k_jn_j)\, e^{n_j\xi z}\Big]\, e^{-I\xi x}\,d\xi, \tag{2.1e}$$

$$\sigma_{z1}(x,z) = \frac{1}{2\pi}\int\limits_{-\infty}^{\infty}\Big[-I\xi\sum_{j=1}^{6} A_j(\bar{C}_{13}+\bar{C}_{36}m_j-\bar{C}_{33}k_jn_j)\, e^{n_j\xi z}\Big]e^{-I\xi x}\,d\xi, \tag{2.1f}$$

$$\tau_{yz1}(x,z) = \frac{1}{2\pi}\int\limits_{-\infty}^{\infty}\Big[\xi\sum_{j=1}^{6} A_j(\bar{C}_{44}m_jn_j+\bar{C}_{45}(k_j+n_j))e^{n_j\xi z}\Big]e^{-I\xi x}\,d\xi, \tag{2.1g}$$

$$\tau_{xz1}(x,z) = \frac{1}{2\pi}\int\limits_{-\infty}^{\infty}\Big[\xi\sum_{j=1}^{6} A_j(\bar{C}_{45}m_jn_j+\bar{C}_{55}(k_j+n_j))e^{n_j\xi z}\Big]e^{-I\xi x}\,d\xi, \tag{2.1h}$$

$$\tau_{xy1}(x,z) = \frac{1}{2\pi}\int\limits_{-\infty}^{\infty}\Big[-I\xi\sum_{j=1}^{6} A_j(\bar{C}_{16}+\bar{C}_{66}m_j-\bar{C}_{36}k_jn_j)e^{n_j\xi z}\Big]e^{-I\xi x}\,d\xi, \tag{2.1i}$$

where $\bar{C}_{ij}$ are the transformed stiffness coefficients of the monoclinic layer, A_j $(j = 1,\ldots,6)$ are the unknowns that will be determined from the boundary conditions of the problem.

The displacement and stress components for the isotropic homogeneous half plane can be written as follows (Yilmaz *et al.* [30])

$$u_2(x,z) = \frac{1}{2\pi}\int\limits_{-\infty}^{\infty}[(B_1+B_2z)e^{|\xi|z}]e^{-i\xi x}\,d\xi, \tag{2.2a}$$

$$v_2(x,z) = \frac{1}{2\pi}\int\limits_{-\infty}^{\infty}[B_3e^{|\xi|z}]e^{-i\xi x}\,d\xi, \tag{2.2b}$$

$$w_2(x,y) = \frac{1}{2\pi}i\int\limits_{-\infty}^{\infty}\left[\frac{|\xi|}{\xi}\left[B_1+\left(-\frac{\kappa_2}{|\xi|}+z\right)B_2\right]e^{|\xi|z}\right]e^{-i\xi x}\,d\xi, \tag{2.2c}$$

$$\frac{\sigma_{x2}(x,y)}{2\mu_2} = -\frac{1}{2\pi}i\int\limits_{-\infty}^{\infty}2\xi\left[B_1e^{|\xi|z}+\left(z-\frac{\kappa_2-3}{2|\xi|}\right)B_2e^{|\xi|z}\right]e^{-i\xi x}\,d\xi, \tag{2.2d}$$

$$\frac{\sigma_{y2}(x,y)}{2\mu_2} = \frac{1}{2\pi}\int_{-\infty}^{\infty}\frac{|\xi|}{\xi}\left[B_2(-3+\kappa_2)e^{|\xi|z}\right]e^{-i\xi x}\,d\xi, \tag{2.2e}$$

$$\frac{\sigma_{z2}(x,y)}{2\mu_2} = \frac{1}{2\pi}i\int_{-\infty}^{\infty}2\xi\left[B_1e^{|\xi|z}+\left(z-\frac{\kappa_2+1}{2|\xi|}\right)B_2e^{|\xi|z}\right]e^{-i\xi x}\,d\xi, \tag{2.2f}$$

$$\frac{\tau_{yz2}(x,y)}{\mu_2} = \frac{1}{2\pi}\int_{-\infty}^{\infty}|\xi|B_3e^{|\xi|z}e^{-i\xi x}\,d\xi, \tag{2.2g}$$

$$\frac{\tau_{xz2}(x,y)}{\mu_2} = \frac{1}{2\pi}\int_{-\infty}^{\infty}2|\xi|\left[B_1e^{|\xi|z}+\left(z-\frac{\kappa_2-1}{2|\xi|}\right)B_2e^{|\xi|z}\right]e^{-i\xi x}\,d\xi, \tag{2.2h}$$

$$\frac{\tau_{xy2}(x,y)}{\mu_2} = -\frac{1}{2\pi}\int_{-\infty}^{\infty}I\xi B_3e^{|\xi|z}e^{-i\xi x}\,d\xi, \tag{2.2i}$$

where μ_2 is the shear modulus of the half plane, $\kappa_2 = 3-4\nu_2$ for the plane strain case and ν_2 is Poisson's ratio of the half plane. The coefficients B_1, B_2 and B_3 will be determined using the boundary conditions of the problem.

3. The boundary conditions and the singular integral equation

The unknown coefficients A_j $(j = 1,\ldots,6)$ and B_l $(l = 1,2,3)$ can be determined from the following boundary conditions of the problem

$$\sigma_{z1}(x,0) = \begin{cases} -p(x) & -a < x < a, \\ 0 & x \le a,\ x \ge a, \end{cases} \tag{3.1a}$$

$$\tau_{xz1}(x,0) = \begin{cases} q(x) & -a < x < a, \\ 0 & x \le a,\ x \ge a, \end{cases} \tag{3.1b}$$

$$\tau_{yz1}(x,0) = 0, \tag{3.1c}$$

$$u_1(x,-h) = u_2(x,-h), \tag{3.1d}$$

$$v_1(x,-h) = v_2(x,-h), \tag{3.1e}$$

$$w_1(x,-h) = w_2(x,-h), \tag{3.1f}$$

$$\sigma_{z1}(x,-h) = \sigma_{z2}(x,-h), \tag{3.1g}$$

$$\tau_{xz1}(x,-h) = \tau_{xz2}(x,-h), \tag{3.1h}$$

$$\tau_{yz1}(x,-h) = \tau_{yz2}(x,-h), \tag{3.1i}$$

where $p(x)$ is the contact stress between the rigid punch and the monoclinic layer on the contact area $(-a,a)$.

Applying the boundary conditions given in Eq. (3.3), the coefficients A_j and B_l can be obtained in terms of the unknown contact stress $p(x)$ and shear stress $q(x)$ as follows

$$A_j = A_j^p \int_{-a}^{a} p(t)e^{I\xi t}\,dt + A_j^q \int_{-a}^{a} q(t)e^{I\xi t}\,dt, \quad j = 1,\ldots,6, \tag{3.2a}$$

$$B_l = B_l^p \int_{-a}^{a} p(t)e^{I\xi t}\,dt + B_l^q \int_{-a}^{a} q(t)e^{I\xi t}\,dt, \quad l = 1,2,3. \tag{3.2b}$$

Since the expressions of A_j^p, A_j^q, B_l^p and B_l^q are too long they are not given here.

To determine the functions $p(x)$ and $q(x)$, the following mixed boundary value conditions should be considered:

$$\frac{\partial w_1(x,0)}{\partial x} = \frac{x}{R}, \qquad -a \le x \le a, \tag{3.3a}$$

$$\frac{\partial u(x,0)}{\partial x} = C|x|, \qquad -b \le x \le b, \tag{3.3b}$$

where C is the slope parameter of the tangential displacement on the stick zone and is an unknown a priori. It must be noted that Eq. (3.3b) ensures the self-similarity condition introduced first by Spence [31]. Substituting the unknowns A_j and B_l into the Eq. (3.3) yields the following second kind Cauchy singular integral equation system

$$\beta_{12}q(x) + \frac{1}{\pi}\int_{-a}^{a} p(t)\left[\frac{\beta_{11}}{t-x} + k_{11}(x,t)\right]dt + \frac{1}{\pi}\int_{-a}^{a} q(t)k_{12}(x,t)\,dt = \frac{x}{R}, \quad -a \le x \le a, \tag{3.4a}$$

$$\beta_{21}p(x) + \frac{1}{\pi}\int_{-a}^{a} p(t)k_{21}(x,t)\,dt + \frac{1}{\pi}\int_{-a}^{a} q(t)\left[\frac{\beta_{22}}{t-x} + k_{22}(x,t)\right]dt = C\,|x|\,, \quad -b \le x \le b. \tag{3.4b}$$

The composite compliance parameters β_{ij}, $i,j = 1,2$ and the kernel functions $k_{ij}(x,t)$, $i,j = 1,2$ are given in the Appendix.

The shear stress in the slip and stick regions can be defined as the following form (Nowell *et al.* [32]):

$$q(x) = \begin{cases} \eta\,\mathrm{sign}(x)p(x), & b < |x| < a \quad \text{(slip regions)}, \\ \eta p(b)\dfrac{x}{b} + q^*(x), & |x| < b \quad \text{(stick region)}, \end{cases} \tag{3.5}$$

here $q^*(x)$ is a perturbation function introduced to correct the shear traction within the stick zone and has to be determined by solving Eq. (3.4b).

Considering (3.5), second integral Eq. (3.4b) becomes as follows

$$\begin{aligned}(3.6)\qquad &\beta_{21}p(x)+\frac{1}{\pi}\int_{-a}^{a}p(t)k_{21}(x,t)\,dt+\frac{\eta}{\pi}\int_{-a}^{-b}p(t)\left[\frac{\beta_{22}}{t-x}+k_{22}(x,t)\right]dt\\ &-\frac{\eta}{\pi}\int_{b}^{a}p(t)\left[\frac{\beta_{22}}{t-x}+k_{22}(x,t)\right]dt\\ &+\frac{1}{\pi}\int_{-b}^{b}q^*(t)\left[\frac{\beta_{22}}{t-x}+k_{22}(x,t)\right]dt\\ &+\frac{1}{\pi}\eta\frac{p(b)}{b}\int_{-b}^{b}\left[\beta_{22}\frac{t}{t-x}+tk_{22}(x,t)\right]dt=C|x|,\quad -b\le x\le b.\end{aligned}$$

Note that the following relation can be written:

$$(3.7)\qquad \int_{-b}^{b}\frac{t}{t-x}\,dt=2b+x\ln\left(\frac{b-x}{b+x}\right).$$

To solve the singular integral Eqs. (3.4a) and (3.6), the contact stress must satisfy the following equilibrium condition:

$$(3.8)\qquad \int_{-\infty}^{\infty}\sigma_z(x,0)\,dx=-\int_{-a}^{a}p(t)\,dt=-P.$$

Introducing the following transformations

$$(3.9)\qquad t=ar,\quad x=as,\quad c=b/a$$

and considering Eq. (3.7), the integral Eqs. (3.4a) and (3.6) become:

$$\begin{aligned}(3.10a)\qquad &\beta_{12}\,q(s)+\frac{1}{\pi}\int_{-1}^{1}p(r)\left[\frac{\beta_{11}}{r-s}+ak_{11}(s,r)\right]dr\\ &+\frac{1}{\pi}\int_{-1}^{1}q(r)ak_{12}(s,r)\,dr=\frac{as}{R},\quad -1\le s\le 1,\end{aligned}$$

$$\beta_{21}\,p(s)+\frac{1}{\pi}\int_{-1}^{1}p(r)ak_{21}(s,r)\,dr+\frac{\eta}{\pi}\int_{-1}^{-c}p(r)\left[\frac{\beta_{22}}{r-s}+ak_{22}(s,r)\right]dr \tag{3.10b}$$
$$-\frac{\eta}{\pi}\int_{c}^{1}p(r)\left[\frac{\beta_{22}}{t-x}+ak_{22}(s,r)\right]dr$$
$$+\frac{1}{\pi}\int_{-c}^{c}q^{*}(r)\left[\frac{\beta_{22}}{r-s}+ak_{22}(s,r)\right]dr$$
$$+\frac{1}{\pi}\eta\frac{p(b)}{c}\beta_{22}\left[2c+sln\frac{c-s}{c+s}\right]$$
$$+\frac{1}{\pi}\eta\frac{p(b)}{b}\int_{-c}^{c}[ark_{22}(s,r)]\,dr=C|as|,\quad -c\le s\le c.$$

It is suitable to introduce another transformation for Eq. (3.10b) as follows:

$$s=c\varphi,\qquad r=c\lambda. \tag{3.11}$$

Thus, the second integral Eq. (3.10b) takes its final form as follows:

$$\beta_{21}p(\varphi)+\frac{1}{\pi}\int_{-1/c}^{1/c}p(\lambda)ack_{21}(\varphi,\lambda)\,d\lambda \tag{3.12}$$
$$+\frac{\eta}{\pi}\int_{-1/c}^{-1}p(\lambda)\left[\frac{\beta_{22}}{\lambda-\varphi}+ack_{22}(\varphi,\lambda)\right]d\lambda$$
$$-\frac{\eta}{\pi}\int_{1}^{1/c}p(\lambda)\left[\frac{\beta_{22}}{\lambda-\varphi}+ack_{22}(\varphi,\lambda)\right]d\lambda$$
$$+\frac{1}{\pi}\int_{-1}^{1}q^{*}(\lambda)\left[\frac{\beta_{22}}{\lambda-\varphi}+ack_{22}(\varphi,\lambda)\right]d\lambda$$
$$+\frac{1}{\pi}\eta\frac{p(b)}{c}\beta_{22}\left[2c+c\varphi ln\frac{1-\varphi}{1+\varphi}\right]$$
$$+\frac{1}{\pi}\eta\frac{p(b)}{b}\int_{-1}^{1}[ac\lambda k_{22}(\varphi,\lambda)]\,d\lambda=C|ac\varphi|,\quad -1\le\varphi\le 1.$$

The unknowns $q^{*}(\lambda)$and $p(\lambda)$ appearing in the integral equations (3.10a) and (3.12) are bound to zero at the ends of their respective intervals. Thus, the solutions can be written as follows:

$$p(r) = F(r)(1-r^2)^{1/2}, \qquad q^*(\lambda) = G(\lambda)(1-\lambda^2)^{1/2}. \tag{3.13}$$

Using Gauss–Chebyshev integration formulas (ERDOGAN [33]), the integral equations (3.10a) and (3.12) and equilibrium condition (3.8) become as follows:

$$\sum_{i=1}^{N} \frac{1}{1-r_i^2}\frac{1}{r_i - s_k}F(r_i) = \frac{1}{R}as_k - M_1(s_k), \qquad k = 1,\dots,N+1, \tag{3.14a}$$

$$\sum_{l=1}^{N} \frac{1}{1-\lambda_l^2}\frac{\beta_{22}}{\lambda_l - \varphi_j}G(\lambda_l) = C|ac\varphi_j| - M_2(\varphi_j), \qquad j = 1,\dots,N+1, \tag{3.14b}$$

$$\sum_{i=1}^{N} \frac{1}{1-r_i^2}F(r_i) = \frac{1}{\pi}P, \tag{3.14c}$$

where the collocation points are chosen as the roots of the Chebyshev polynomials of the second kind given below:

$$r_i = \cos\left(\frac{i}{N+1}\pi\right), \qquad i = 1,\dots,N, \tag{3.15a}$$

$$s_k = \cos\left(\frac{2k-1}{2(N+1)}\pi\right), \qquad k = 1,\dots,N+1, \tag{3.15b}$$

$$\lambda_l = \cos\left(\frac{l}{N+1}\pi\right), \qquad l = 1,\dots,N, \tag{3.15c}$$

$$\varphi_j = \cos\left(\frac{2z-1}{2(N+1)}\pi\right), \qquad j = 1,\dots,N+1, \tag{3.15d}$$

$$M_1(s_k) = \beta_{12}q(s_k) + \frac{1}{\pi}\int_{-1}^{1} q(r)ak_{12}(s_k, r)\,dr, \tag{3.15e}$$

$$\begin{aligned} M_2(\varphi_j) = {} & \beta_{21}p(\varphi_j) + \frac{1}{\pi}\int_{-1/c}^{1/c} p(\lambda)ack_{21}(\varphi_j,\lambda)\,d\lambda \\ & + \frac{\eta}{\pi}\int_{-1/c}^{-1} p(\lambda)\left[\frac{\beta_{22}}{\lambda-\varphi_j} + ack_{22}(\varphi_j,\lambda)\right]d\lambda \\ & - \frac{\eta}{\pi}\int_{1}^{1/c} p(\lambda)\left[\frac{\beta_{22}}{\lambda-\varphi_j} + ack_{22}(\varphi_j,\lambda)\right]d\lambda \\ & + \frac{1}{\pi}\eta\frac{p(b)}{c}\beta_{22}\left[2c + c\varphi_j ln\frac{1-\varphi_j}{1+\varphi_j}\right] + \frac{1}{\pi}\eta\frac{p(b)}{b}\int_{-1}^{1}[ac\lambda k_{22}(\varphi_j,\lambda)]\,d\lambda. \end{aligned} \tag{3.15f}$$

Note that, both in Eqs. (3.14a) and (3.14b) there are one more equation to find the unknowns $F(r_i)$ and $G(\lambda_l)$. The reason for this is that the problem at hand involves only normal loading which makes the problem symmetric, it is presumed that the left and the right contact boundaries are equal. Hence an equation can be omitted from the numerical algebraic system of equations. Although any equation can be omitted from the system of equations, it is recommended to select "N" as an even number and the equation corresponding to "$k = \frac{N}{2} + 1$" can be omitted from Eq. (3.14a) [33]. On the other hand, the extra equation in Eq. (3.14a) must be extracted and used as a control equation with (3.14c) to find the contact width a and the stick zone c.

The slope parameter of the tangential displacement on the stick zone C is also unknown and the following extra control equation is essential to solve the problem:

$$G(+1) = 0 \quad \text{or} \quad G(-1) = 0. \tag{3.16}$$

This equation ensures the continuity of surface tangential strain as introduced by NOWELL *et al.* [34]. The reader is referred to GULER *et al.* [35] for further explanation. Here $G(-1)$ and $G(+1)$can be calculated as follows (KRENK [36])

$$G(+1) = \sum_{l=1}^{N} \cot\left(\frac{l}{N+1}\frac{\pi}{2}\right) \sin\left(\frac{N}{N+1} l\pi\right) G(\lambda_l), \tag{3.17a}$$

$$G(-1) = \sum_{l=1}^{N} \cot\left(\frac{l}{N+1}\frac{\pi}{2}\right) \sin\left(\frac{N}{N+1} l\pi\right) G(\lambda_{N+1-l}). \tag{3.17b}$$

Due to the unknowns a, c and C the algebraic equation system is nonlinear and an iterative method must be used.

To determine the unknowns $F(r_i)$, $G(\lambda_l)$, the contact width a, the stick zone c and the slope C, the following steps are applied:

1. Make an initial guess for the contact width a. A rapid approximation can be employed by the classical Hertzian contact solution, i.e. $a = \sqrt{\frac{2PR(1-\nu_2)}{\pi\mu_2}}$.

2. Neglecting the term $M_1(s_k)$, i.e. $q(s_k)$, in (3.14a) , solve Eq. (3.14a) , find $F(r_i)$ and the control the equilibrium condition (3.14c).

3. If the equilibrium condition (3.14c) is satisfied in the desired accuracy, go to the next step. If not back to the previous step 1.

4. Fitting a function for $F(r_i)$ and obtain $p(r)$ using Eq. (3.13). Thus, the values of $M_2(z_j)$ in Eq. (3.14b) can be determined.

5. Extract any one equation from Eq. (3.14b) and use this equation as a control equation with Eq. (3.16) to determine the parameters c and C.

6. Make an initial guess for the stick zone c and the slope C, solve Eq. (3.14b), find $G(\lambda_l)$. For the stick zone half-length, one may use the approximate relation

based on the classical partial slip contact problem, i.e. $\frac{K(\sqrt{1-c^2})}{K(c)} = \frac{1-2\nu_2}{2(1-\nu_2)\eta}$. The slop parameter, C, can also be predicted by means of the classical partial slip contact problem, i.e. $C = \frac{\pi\eta}{RcK(c)}$.

7. If the control equations are satisfied in the desired accuracy, go to the next step. If not back to the previous step 6.

8. Fitting a function for $G(\lambda_l)$ and obtain $q^*(\lambda)$ using Eq. (3.13). Hence, $M_1(s_k)$, i.e. $q(s_k)$ can be determined with the Eq. (3.5).

9. Back to step 1 and start a new iteration without neglecting the $M_1(s_k)$ in (3.14a).

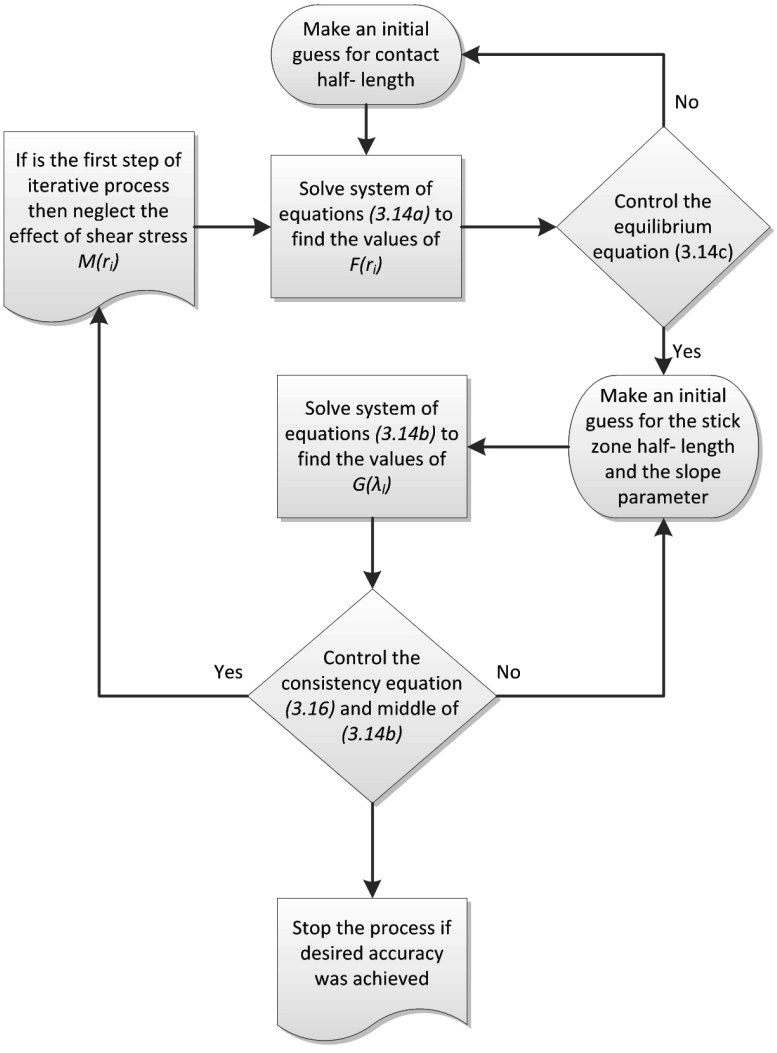

FIG. 2. The flowchart diagram for the numerical solution procedure.

10. In the step 6, use the determined value of c and C from the first iteration as an initials.

11. Continue to the iteration until desired convergences are achieved in c and C between the iterations.

In order to fit the unknown functions $F(r)$ and $G(\lambda)$, one may expand these functions in terms of the Chebyshev polynomial of the second kind, i.e. $F(r) = \sum_{i=0}^{N-1} \Psi_i U_i(r)$ and $G(\lambda) = \sum_{i=0}^{N-1} \Omega_i U_i(\lambda)$. The coefficients Ψ_i and Ω_i are then determined as [33]:

$$\begin{aligned} \Psi_i &= \frac{2}{N+1} \sum_{j=1}^{N} \left(1 - r_j^2\right) U_i(r_j) F(r_j) \quad (i = 1, \ldots, N-1), \\ \Omega_i &= \frac{2}{N+1} \sum_{j=1}^{N} (1 - \lambda_j^2) U_i(\lambda_j) G(\lambda_j) \quad (i = 1, \ldots, N-1). \end{aligned} \tag{3.18}$$

After determining the normal and tangential tractions on the surface and the parameters a, c and C, the in-plane stress at the surface of the monoclinic coated half plane can be determined. The numerical solution procedure is also given as a flowchart in Fig. 2 for more clarity.

4. Results and discussions

In what follows and unless noted otherwise, the material employed for the monoclinic layer in the problem considered is Glass/Epoxy as given in Table 1. ÇÖMEZ *et al.* [29] investigated the partial slip contact problem between a rigid punch and a monoclinic half plane. The solution of the mentioned problem can

Table 1. Material properties of polymer and metal-matrix unidirectional composites [37].

Material property (GPa)	GI/Ep	Gr/Ep (T300/934)	Gr/Ep (P75/934)	B/Al	Gr/Al
E_{11}	42.7	144.8	243.0	227.5	402.6
E_{22}	11.7	10.3	7.2	137.9	24.1
E_{33}	11.7	10.3	7.2	137.9	24.1
ν_{12}	0.27	0.3	0.33	0.24	0.29
ν_{13}	0.27	0.3	0.33	0.24	0.29
ν_{33}	0.55	0.5	0.49	0.4	0.45
G_{12}	8.238	5.515	3.929	55.152	16.75
G_{13}	8.238	5.515	3.929	55.152	16.75
G_{23}	3.778	3.447	2.406	49.2444	8.34

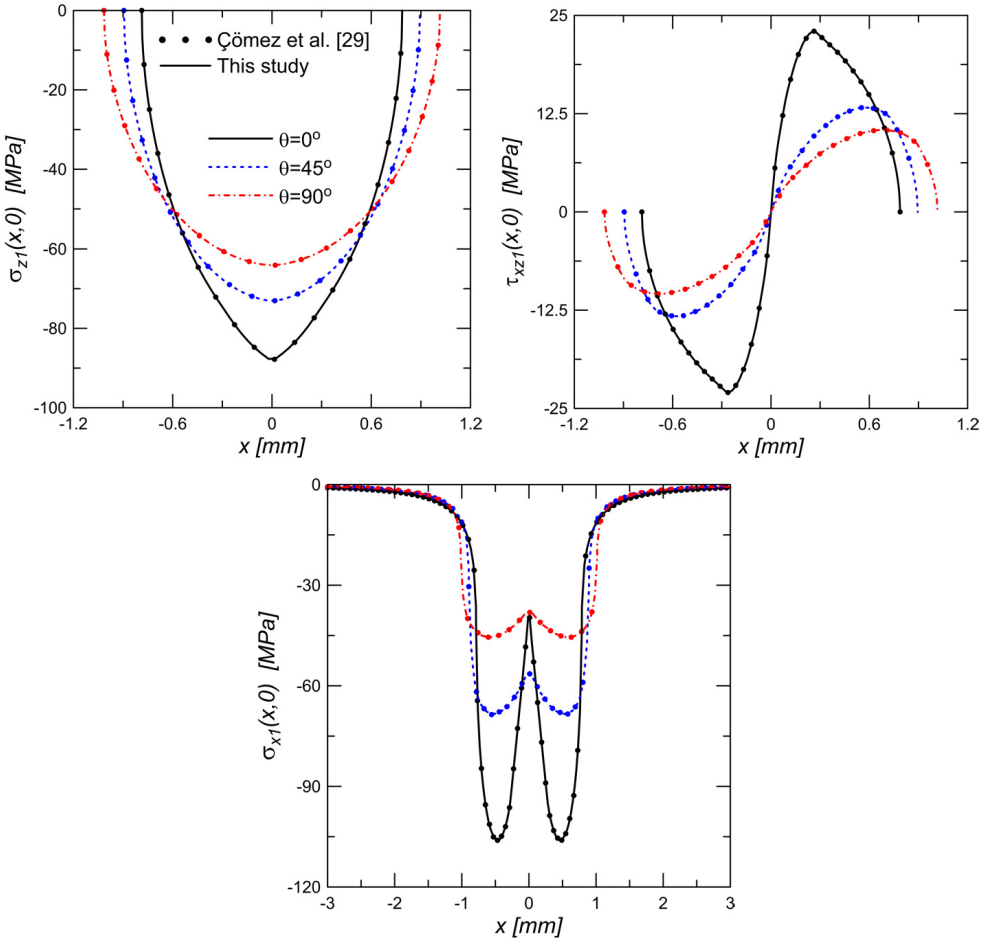

FIG. 3. Validation of the stresses for a monoclinic half plane indented by a cylindrical punch; comparison with ÇÖMEZ *et al.* [29] ($\eta = 0.3$, $R = 0.1\,\mathrm{m}$, $P = 100\,\mathrm{kN/m}$, $h \to \infty$, material Gl/Ep).

be recovered as a limiting case of the current study. The results shown in Fig. 3 indicate that the stress components of current study meet very well with those given by ÇÖMEZ *et al.* [29] as the thickness of the monoclinic layer tends to infinity.

As an important parameter, Fig. 4 demonstrates the effect of orientation of the material principal directions on the stress field. In fact, the contribution of material anisotropy can be inferred as the effect of relative stiffness along the indentation path to the tangential direction. For the case $\theta = 0°$, the stiffness of the Glass/Epoxy along the indentation depth is about one-fourth that of the tangential direction, whereas for the case $\theta = 90°$, the stiffness is equal in both

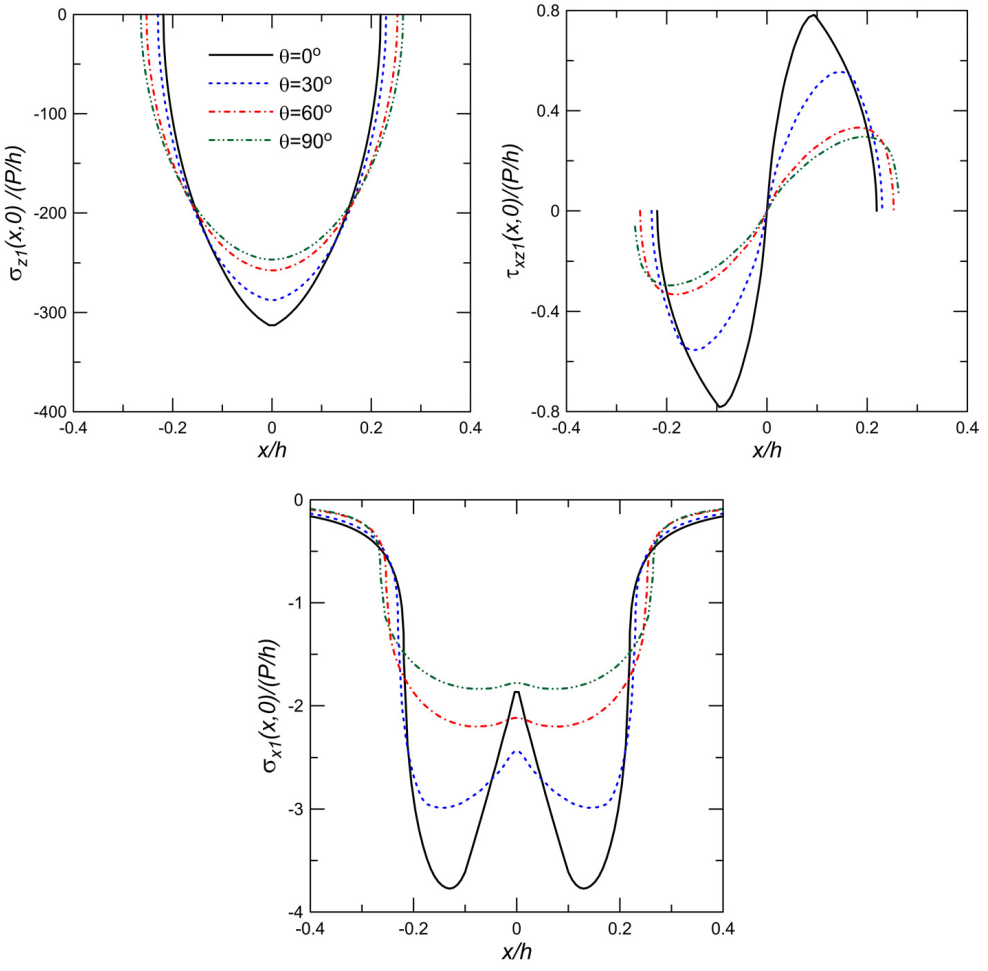

FIG. 4. Effect of fiber angle θ on the surface stresses ($\eta = 0.3$, $R/h = 10$, $\mu_2/(P/h) = 500$, $\kappa = 2$).

directions. Thus, one may anticipate that the contact pressure would be much higher for the case $\theta = 0°$ compared to other cases. Noting Columb's friction law, see Eq. 6, the distribution of the shear stress is mainly proportional to the contact pressure therefore the highest values corresponding to the case $\theta = 0°$. Also, the stick area, b, shrinks as the material becomes more compliant along the tangential direction. The normal indentation of the system by a rigid punch can result in compressive strain along the contact surface. Table 2 verifies that the value of slop parameter, C, is negative for different fiber angle orientations. This tangential compressive strain produces a compressive in plane stress as shown in Fig. 4. Note that the shear stress is an odd function of the horizontal

Table 2. The variation of the contact width a, stick zone c and slop parameter C with the fiber angle θ and friction coefficient η ($\eta = 0.3$, $R/h = 10$, $\mu_2/(P/h) = 500$, $\kappa = 2$).

θ	a/h	c	C
0	0.2191	0.4325	−47.1847
30°	0.2302	0.7499	−27.0962
45°	0.2416	0.8882	−20.3141
60°	0.2532	0.9333	−17.1913
90°	0.2645	0.9452	−15.9009

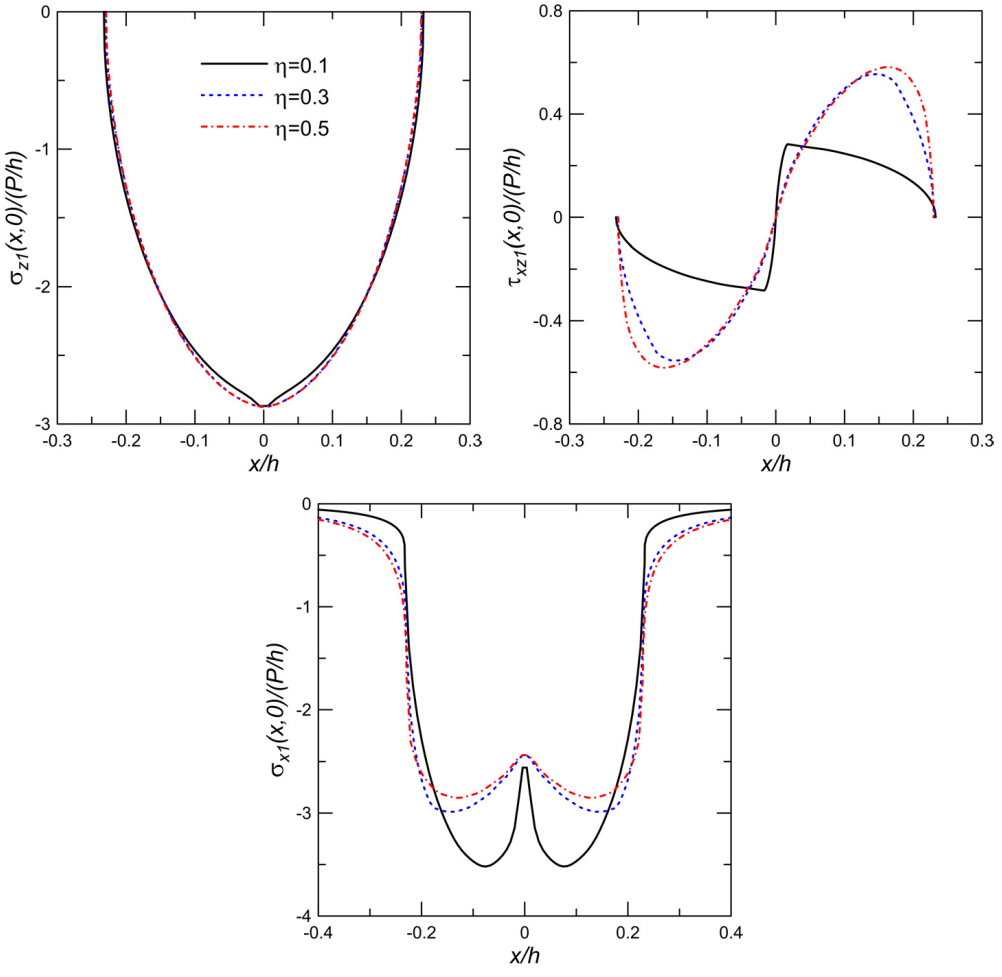

FIG. 5. Effect of friction coefficient η on the surface stresses ($\theta = 30°$, $R/h = 10$, $\mu_2/(P/h) = 500$, $\kappa = 2$).

coordinate since the particles move toward the center of the contact region, i.e. the particles on the right side of the contact tend to move to the left while the opposite is true for the particles on the left side of the contact. Since the most stiff case corresponds to $\theta = 0°$, the particles are more constraint to move toward the contact center and results in the maximum shear stress. Also, the increase of the in-plane stress at the middle part of the contact region might be attributed to the tangential strain field, of the form $\varepsilon_{xx} = C|x|$, $-c < x < c$, in the stick region (self- similarity condition, see [31]).

For the special case $\theta = 30°$, the effect of the friction coefficient on the surface stresses is given in Fig. 5. The well-known Goodman approximation which

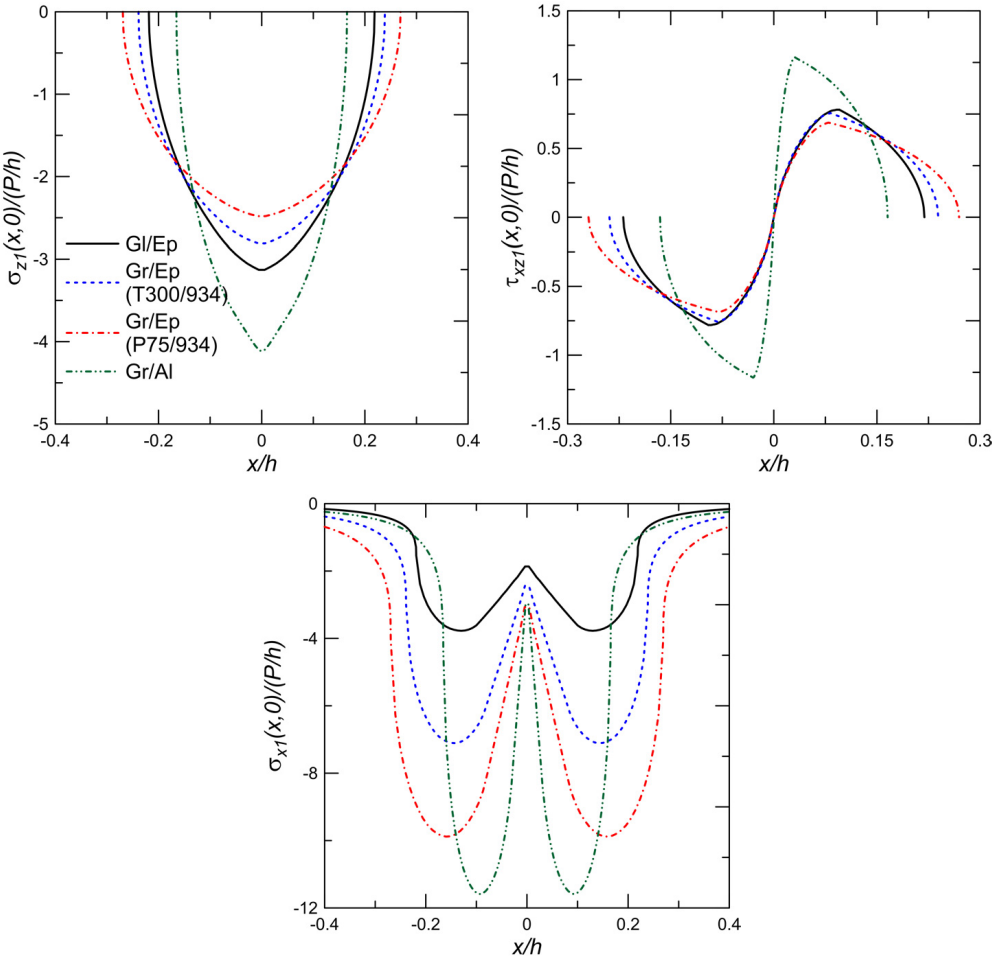

FIG. 6. Effect of material types on the surface stresses ($\theta = 0$, $\eta = 0.3$, $R/h = 10$, $\mu_2/(P/h) = 500$, $\kappa = 2$).

neglects the effect of the shear traction on the contact stress can be adapted to the current results. As the friction coefficient increases, it can be observed that the shear traction follows significant changes whereas the contact pressure has negligible variations. Also, a higher value of the friction coefficient restrains the relative tangential displacement at the contact surface which in turn increases the stick zone length. The shear stress within the slip area is directly proportional to the friction coefficient as shown in Fig. 5. The surface in-plane stress arises due to surface tractions such that the contact pressure induces a compressive tangential strain while the anti-symmetric shear stress imposes a tensile tangential strain at the contact center and a compressive one at the contact edges. Hence, as the shear stress increases by elevating the friction coefficient, the absolute value of in-plane stress reduces at the contact center whilst increases near the contact edges.

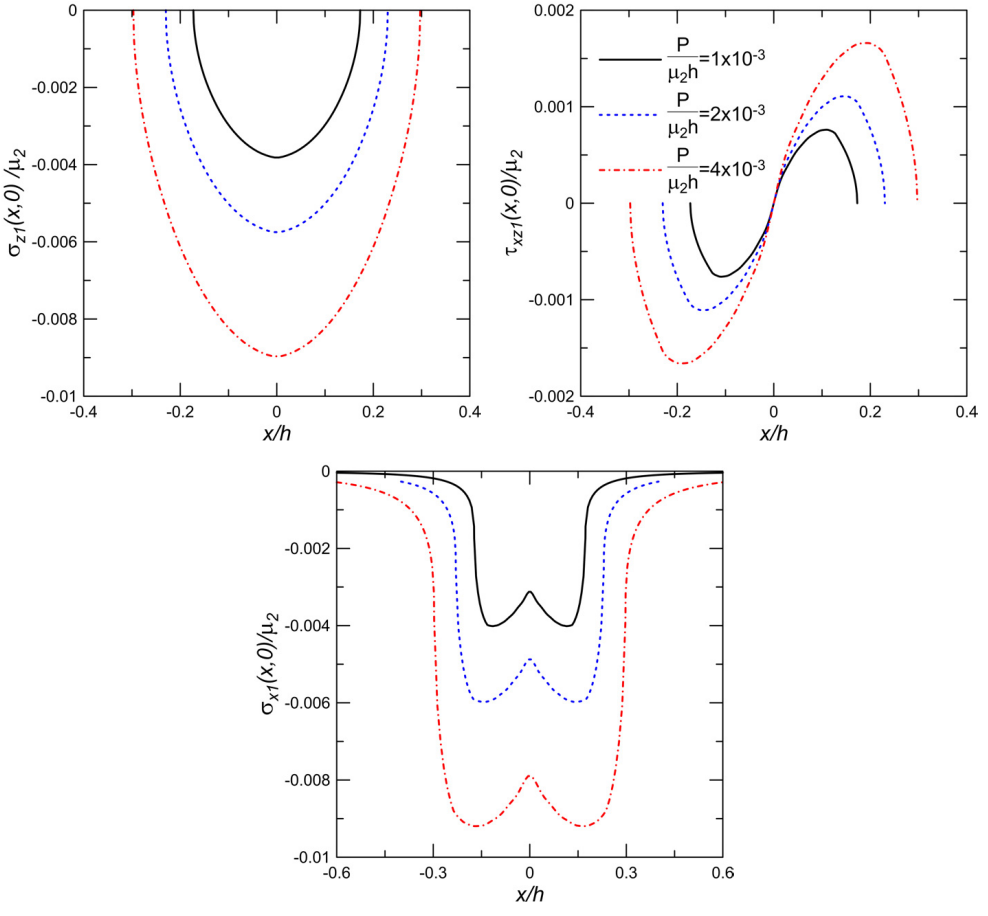

FIG. 7. Effect of indentation load P on the surface stresses ($\theta = 30^\circ$, $\eta = 0.3$, $R/h = 10$, $\kappa = 2$).

Note that there is a dramatic decrease in the stick region for the lower values of the friction coefficient (for example $\eta = 0.1$). This can be explained as the slip region increases when there is less friction hence the stick region becomes less and less. If the friction coefficient decreases further to zero (a frictionless case) then there will be no stick region.

Figure 6 presents the distribution of the surface stresses for different types of orthotropic materials as given in Table 1. It can be observed that Br/Al gives the highest contact pressure while the opposite is true for Gr/Ep(P75/934). This behavior depends on two factors, first the stiffness ratio of penetration direction to the tangential direction (i.e. E_z/E_x); second the relative stiffness

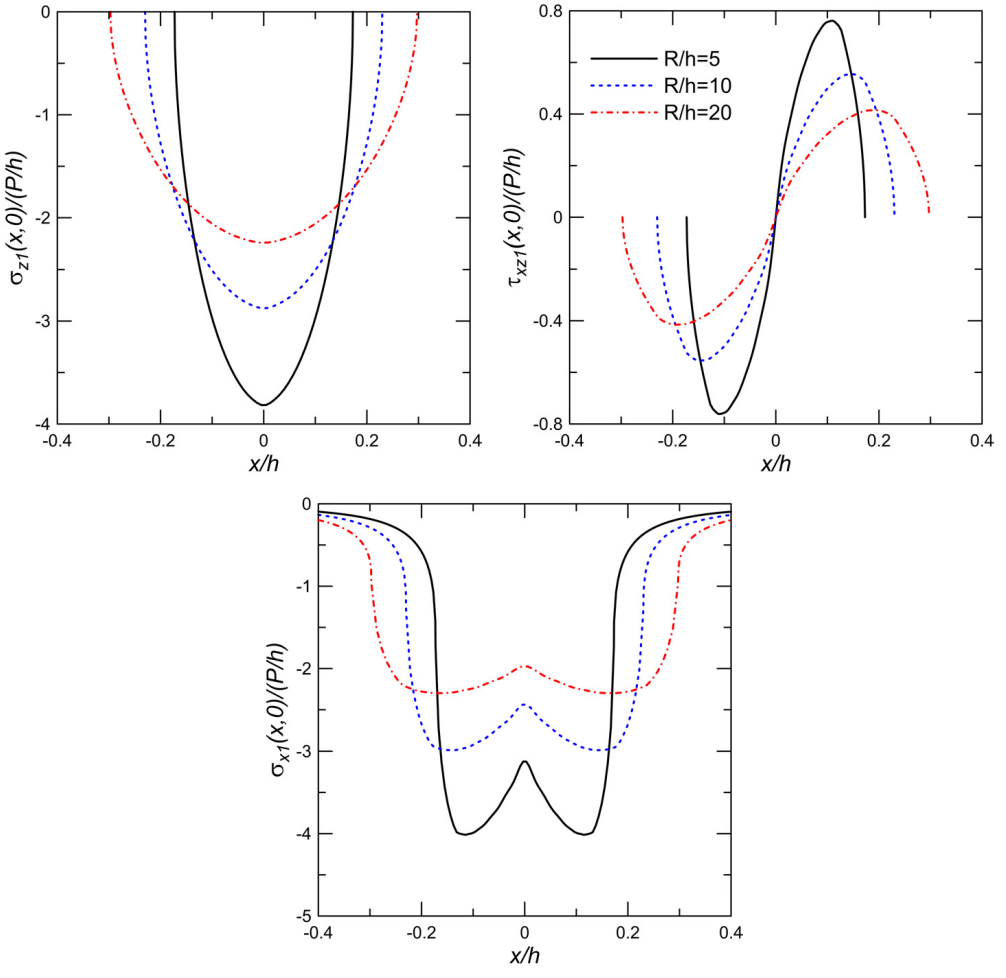

FIG. 8. Effect of punch radius R on the surface stresses ($\theta = 30^\circ$, $\eta = 0.3$, $\mu_2/(P/h) = 500$, $\kappa = 2$).

of the anisotropic coating to the isotropic substrate ($\sqrt{E_z E_x}/\mu_2$). As stated before, if the material possesses a higher value of E_z/E_x then its penetration response will be a smaller contact area or equivalently an intensified contact pressure. A similar argument can be concluded for the effect of $\sqrt{E_z E_x}/\mu_2$ on the contact pressure. In view of this, Br/Al has the maximum value of $E_z/E_x = 0.6$ and $\sqrt{E_z E_x}/\mu_2 = 3.5$ at the same time. For Gr/Ep(P75/934), the mentioned parameters decrease to $E_z/E_x = 0.3$ and $\sqrt{E_z E_x}/\mu_2 = 0.8$. Other material types may be sorted by a compromise between the values of E_z/E_x and $\sqrt{E_z E_x}/\mu_2$. Also, the ratio of stick to slip area increases as the material gets stiffer along the tangential direction. At the same time, the compressive in-plane stress builds up for a material possessing larger stiffness along the tangential direction.

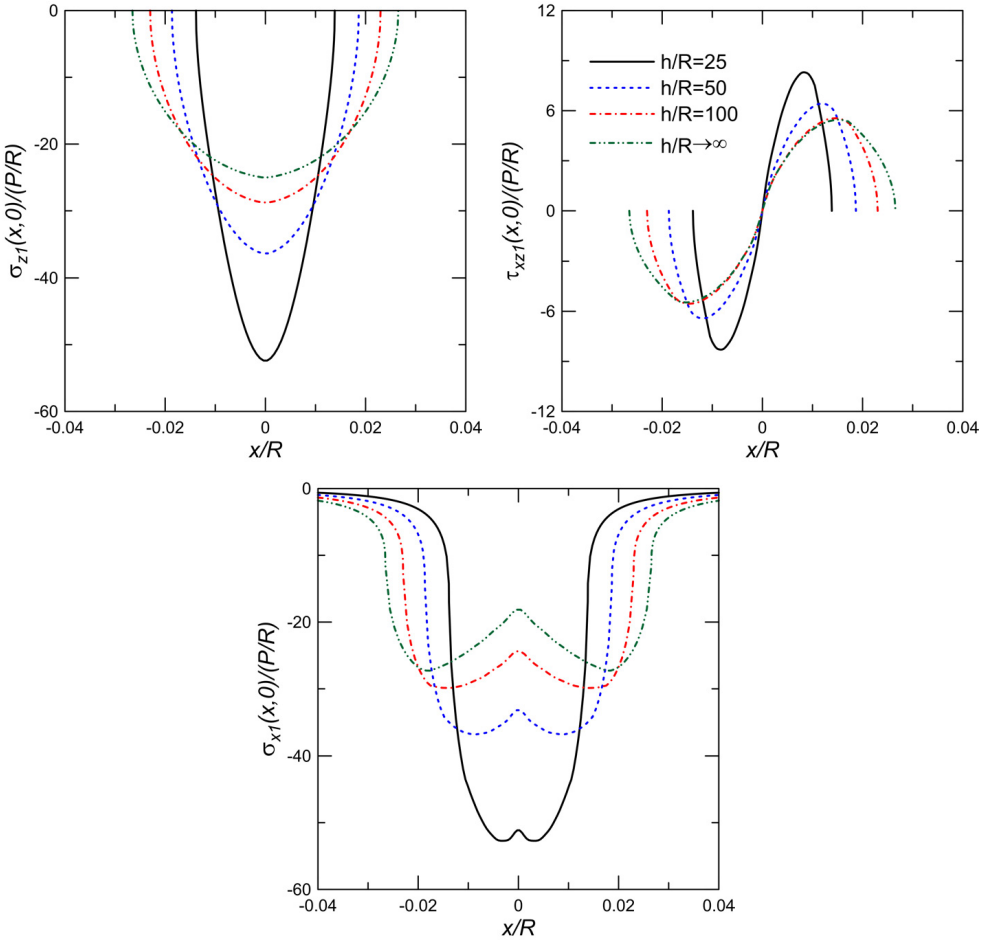

FIG. 9. Effect of layer thickness h on the surface stresses ($\eta = 0.3$, $\theta = 30°$, $\mu_2/(P/R) = 5000$, $\kappa = 2$).

Dependence of surface stresses to the applied load is given in Fig. 7. From the classical Hertzian contact problem, the contact half-length and the maximum contact pressure are proportional to the square root of applied load. In other words, if the load changes by a factor of n then both the contact half-length and the maximum contact pressure change by a factor of $\sqrt{n}$. For an anisotropic system, the results indicate that the proportionality factor of the contact half-length is slightly smaller than $\sqrt{n}$ but the proportionality factor of the maximum contact pressure is larger than $\sqrt{n}$. Both the shear traction and the surface in-plane stress significantly increase by elevation of an applied load.

Figures 8 and 9 study the effects of a punch radius and the coating thickness over the surface stresses, respectively. As the radius of a punch increases, a larger portion of it comes into contact with the coating surface. In turn, the

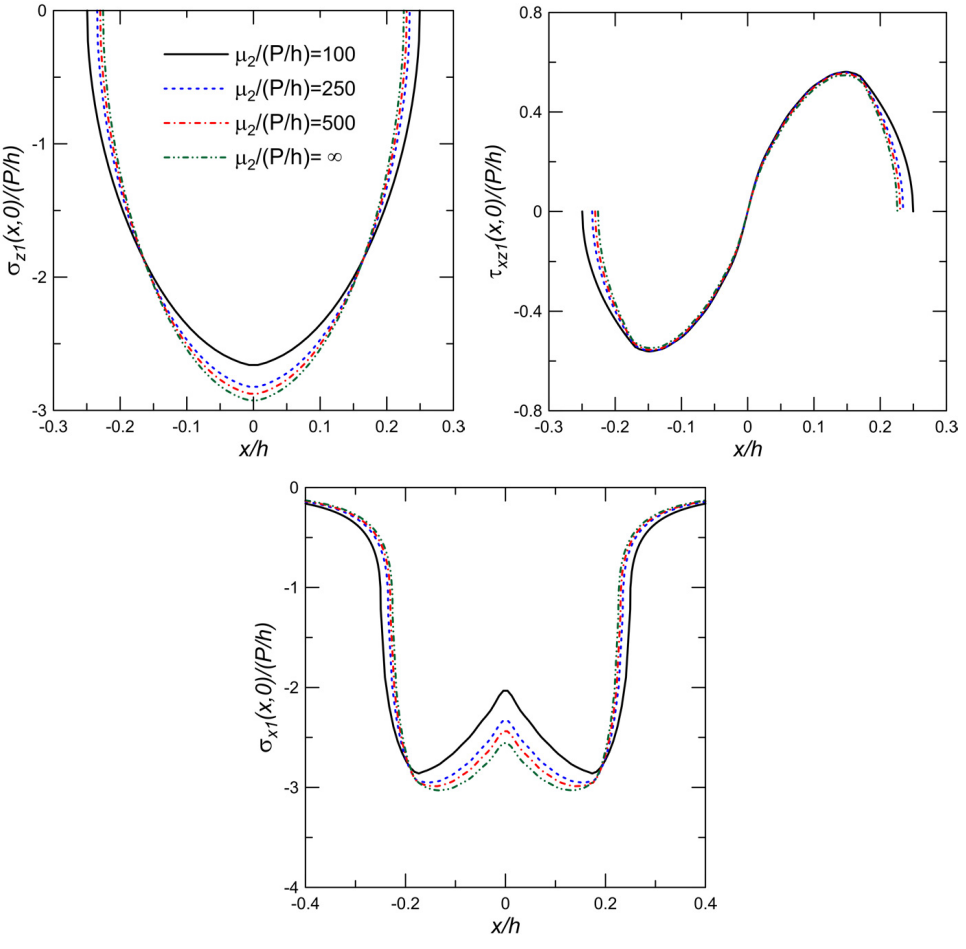

FIG. 10. Effect of shear modulus of the half plane μ_2 on the surface stresses ($\theta = 30°$, $\eta = 0.3$, $R/h = 10$, $\kappa = 2$).

load distributes on a wider area and the contact pressure distribution becomes smoother. Both the shear traction and the surface in-plane stress obey the same rule as shown in Fig. 8. Regarding Fig. 9, the absolute value of surface stresses decreases as the thickness of Gl/Ep coating gradually increases. For a very thin coating, the contact pressure builds up due to the relative rigidity of the coating to the substrate.

The effect of substrate stiffness on the surface stresses is described in Fig. 10. For a constant coating stiffness, if the substrate become more rigid then the surface penetration decreases. Thus, the contact pressure is maximal for a completely rigid substrate. Since the surface tangential deformation of the coating is not sensitive to the substrate rigidity, the surface shear traction slightly changes within the slip area. For a rigid substrate, higher contact pressure results in more compressive in-plane stress at the contact center and lower in-plane stress near the contact edges.

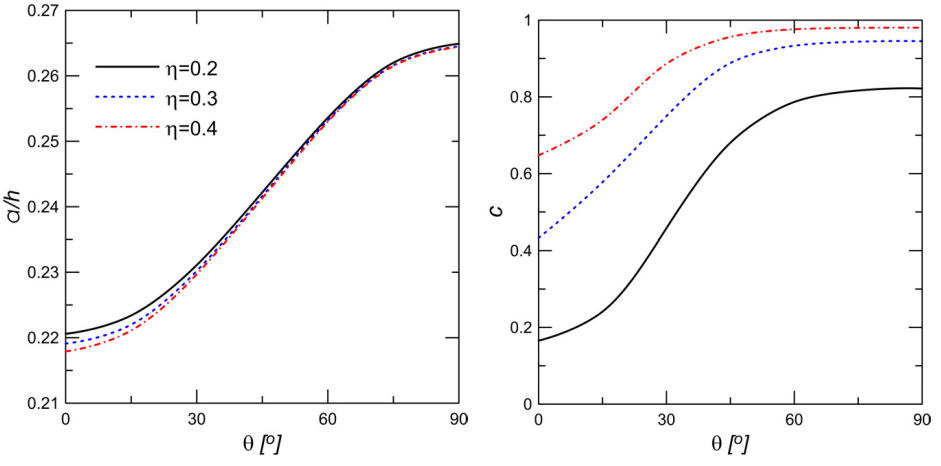

FIG. 11. Variations of the contact area a and stick zone $c = b/a$ for various values of fiber angle θ and the friction coefficient η, ($R/h = 10$, $\mu_2/(P/h) = 500$, $\kappa = 2$).

Variations of contact and the stick zones half-length versus the coating fiber angle is given in Fig. 11 for various values of the friction coefficient. It can be observed that both contact and stick zone increase to a cetrain extent. As the fiber angle approches $\theta = 90°$, variation of the contact zone is up to 20% whereas the stick zone may increase by a factor of 4.8, 2.2 and 1.5 corresponding to $\eta = 0.2$, $\eta = 0.3$ and $\eta = 0.4$, respectively.

5. Conclusions

This paper established the generalized 2D contact problem between a rigid punch and a monoclinic layer/substrate system. The partial slip boundary condi-

tion was adapted on the contact surface. The transformed equilibrium equations for the anisotropic layer were solved in the Fourier domain. A comprehensive numerical stduy was carried out for the effective material and geometric parameters. Some concluding remarks are given below:

1. Proper adjustment of the fiber angle of the coating can be employed to tolerate the severe surface stresses.
2. The friction coefficient has a minimal effect on the contact pressure whereas substantially affects the shear traction distribution. Thus, the contact pressure can be obtained using the uncoupled approximation.
3. When the substrate stiffness increases (while the coating material is fixed) the contact pressure builds up and the contact area recedes. The similar argument holds when the substrate is fixed and the stiffness of the coating material increases.
4. For the Hertzian contact, if the load is monotonicaly increasing then the contact half- length is increased by a factor of the square root of the applied load. However, for the anisotropic system, if the load is monotonicaly increasing then the contact half- length is increased by a factor more than the square root of the applied load.
5. The effect of the fiber angle variation on the stick zone length (80% variation) is more pronounced than on the contact length (20% variation).

Appendix

The composite compliance parameters β_{ij}, $i,j=1,2$ and the kernel functions $k_{ij}(x,t)$, $i,j=1,2$ are defined here:

$$k_{11}(x,t)=\int_0^\infty [M_{11}(\xi)-\beta_{11}]\sin\xi(t-x)\,d\xi, \tag{A.1}$$

$$k_{12}(x,t)=\int_0^\infty [M_{12}(\xi)-\beta_{12}]\cos\xi(t-x)\,d\xi, \tag{A.2}$$

$$k_{21}(x,t)=\int_0^\infty [M_{21}(\xi)-\beta_{21}]\cos\xi(t-x)\,d\xi, \tag{A.3}$$

$$k_{22}(x,t)=\int_0^\infty [M_{22}(\xi)-\beta_{22}]\sin\xi(t-x)\,d\xi, \tag{A.4}$$

where

$$
\begin{aligned}
M_{11}(\xi) &= I\xi \sum_{j=1}^{6} m_j A_j^p, \quad M_{12}(\xi) = \xi \sum_{j=1}^{6} m_j A_j^q, \\
M_{21}(\xi) &= -I\xi \sum_{j=1}^{6} A_j^p, \quad M_{22}(\xi) = \xi \sum_{j=1}^{6} A_j^q
\end{aligned} \tag{A.5}
$$

and

$$
\begin{aligned}
\beta_{11} &= \lim_{\xi\to\infty} M_{11}(\xi), \quad \beta_{12} = \lim_{\xi\to\infty} M_{12}(\xi), \\
\beta_{21} &= \lim_{\xi\to\infty} M_{21}(\xi), \quad \beta_{22} = \lim_{\xi\to\infty} M_{22}(\xi).
\end{aligned} \tag{A.6}
$$

Conflict of interest

The authors declare that they have no conflict of interest.

References

1. M. Ciavarella, G. Demelio, *A review of analytical aspects of fretting fatigue, with extension to damage parameters, and application to dovetail joints*, International Journal of Solids and Structures, **38**, 10–13, 1791–811, 2001.
2. R. Rajasekaran, D. Nowell, *Fretting fatigue in dovetail blade roots: experiment and analysis*, Tribology International, **39**, 10, 1277–1285, 2006.
3. J. Juoksukangas, A. Lehtovaara, A. Mäntylä, *Experimental and numerical investigation of fretting fatigue behavior in bolted joints*, Tribology International, **103**, 440–448, 2016.
4. C. Jiménez-Peña, R.H. Talemi, B. Rossi, D. Debruyne, *Investigations on the fretting fatigue failure mechanism of bolted joints in high strength steel subjected to different levels of pre-tension*, Tribology International, **108**, 128–140, 2017.
5. J. Chao, *Fretting-fatigue induced failure of a connecting rod*, Engineering Failure Analysis, **96**, 186–201, 2019.
6. T. Rauert, J. Herrmann, P. Dalhoff, M. Sander, *Fretting fatigue induced surface cracks under shrink fitted main bearings in wind turbine rotor shafts*, Procedia Structural Integrity, **2**, 3601–3609, 2016.
7. D. Houghton, P.M. Wavish, E.J. Williams, S.B. Leen, *Multiaxial fretting fatigue testing and prediction for splined couplings*, International Journal of Fatigue, **31**, 11–12, 1805–1815, 2009.
8. J. Ding, S.B. Leen, E.J. Williams, P.H. Shipway, *Finite element simulation of fretting wear-fatigue interaction in spline couplings*, Tribology-Materials, Surfaces & Interfaces, **2**, 1, 10–24, 2008.

9. M. Buciumeanu, A.S. Miranda, A.C. Pinho, F.S. Silva, *Design improvement of an automotive-formed suspension component subjected to fretting fatigue*, Engineering Failure Analysis, **14**, 5, 810–821, 2007.

10. H. Mohrbacher, J.P. Celis, J.R. Roos, *Laboratory testing of displacement and load induced fretting*, Tribology International, **28**, 5, 269–2678, 1995.

11. Z.R. Zhou, L. Vincent, *Effect of external loading on wear maps of aluminium alloys*, Wear, **162**, 619–623, 1993.

12. L. Vincent, Y. Berthier, M. Godet, *Testing methods in fretting fatigue: a critical appraisal. Standardization of fretting fatigue test methods and equipment*, ASTM International, 33-33-16, 1992.

13. M. Kuno, R.B. Waterhouse, D. Nowell, D.A. Hills, *Initiation and growth of fretting fatigue cracks in the partial slip regime*, Fatigue & Fracture of Engineering Materials & Structures, **12**, 5, 387–398, 1989.

14. L. Gallego, D. Nélias, *Modeling of fretting wear under gross slip and partial slip conditions*, Journal of Tribology, **129**, 3, 528–535, 2007.

15. I. Goryacheva, P. Rajeev, T. Farris, *Wear in partial slip contact*, Journal of Tribology, **123**, 4, 848–856, 2000.

16. H. Andresen, D.A. Hills, J.R. Barber, J. Vazquez, *Frictional half-plane contact problems subject to alternating normal and shear loads and tension in the steady state*, International Journal of Solids and Structures, **168**, 166–171, 2019.

17. H. Andresen, D.A. Hills, J.R. Barber, J. Vázquez, *Steady state cyclic behaviour of a half-plane contact in partial slip subject to varying normal load, moment, shear load, and moderate differential bulk tension*, International Journal of Solids and Structures, **82**, 156–161, 2020.

18. L. Galin, G. Gladwell, *Contact Problems*, Springer, Dordrecht, Netherlands, 2008.

19. C. Bagault, D. Nélias, M. Baietto, *Contact analyses for anisotropic half space: effect of the anisotropy on the pressure distribution and contact area*, Journal of Tribology, **134**, 3, 2012.

20. H. Fan, L. Keer, *Two-dimensional contact on an anisotropic elastic half-space*, Journal of Applied Mechanics, **61**, 2, 250–255, 1994.

21. L.M. Brock, H.G. Georgiadis, *Multiple-zone sliding contact with friction on an anisotropic thermoelastic half-space*, International Journal of Solids and Structures, **44**, 9, 2820–2836, 2007.

22. T. Hayashi, H. Koguchi, N. Nishi, *Contact analysis for anisotropic elastic materials considering surface stress and surface elasticity*, Journal of the Mechanics and Physics of Solids, **61**, 8, 1753–1767, 2013.

23. L. Rodríguez-Tembleque, F.C. Buroni, R. Abascal, A. Sáez, *3D frictional contact of anisotropic solids using BEM*, European Journal of Mechanics-A/Solids, **30**, 2, 95–104, 2011.

24. L. Rodríguez-Tembleque, M. Aliabadi, R. Abascal, *Anisotropic contact and wear simulation using boundary elements*, Key Engineering Materials, **618**, 73–98, 2014.

25. Y. ALINIA, M.A. GÜLER, *On the fully coupled partial slip contact problems of orthotropic materials loaded by flat and cylindrical indenters*, Mechanics of Materials, **114**, 119–133, 2017.

26. J. SU, L.L KE, Y.S. WANG, *Two-dimensional fretting contact analysis of piezoelectric materials*, International Journal of Solids and Structures, **73**, 41–54, 2015.

27. J. SU, L.L KE, Y.S. WANG, *Two-dimensional fretting contact of piezoelectric materials under a rigid conducting cylindrical punch*, Journal of Mechanics of Materials and Structures, **11**, 5, 535–558, 2016.

28. J. SU, L.L KE, Y.S. WANG, *Fretting contact of a functionally graded piezoelectric layered half-plane under a conducting punch*, Smart Materials and Structures, **25**, 2, 025014, 2016.

29. İ ÇÖMEZİ Y. ALINIA, M.A. GÜLER, S. EL-BORGI, *Partial slip contact analysis for a monoclinic half plane*, Mathematics and Mechanics of Solids, **26**, 3, 401–421, 2021.

30. K.B. YILMAZ, İ ÇÖMEZİ M.A. GÜLER, B.O. YILDIRIM, *Sliding frictional contact analysis of a monoclinic coating/isotropic substrate system*, Mechanics of Materials, **137**, 103–132, 2019.

31. D. SPENCE, *Self similar solutions to adhesive contact problems with incremental loading*, Proceedings of the Royal Society of London, Series A, Mathematical and Physical Sciences, **305**, 1480, 55–80, 1968.

32. D. NOWELL, D.A. HILLS, A. SACKFIELD, *Contact of dissimilar elastic cylinders under normal and tangential loading*, Journal of the Mechanics and Physics of Solids, **36**, 1, 59–75, 1988.

33. F. ERDOGAN, *Mixed boundary value problems*, Mechanics Today, S. Nemat-Nasser [ed.], **4**, 1–86, 2013.

34. D. NOWELL, D.A. HILLS, *Tractive rolling of dissimilar elastic cylinders*, International Journal of Mechanical Sciences, **30**, 6, 427–439, 1988.

35. M.A. GÜLER, S. ADIBNAZARI, Y. ALINIA, *Tractive rolling contact mechanics of graded coatings*, International Journal of Solids and Structures, **49**, 6, 929–945, 2012.

36. S. KRENK, *On the use of the interpolation polynomial for solutions of singular integral equations*, Quarterly of Applied Mathematics, **32**, 4, 479–484, 1975.

37. W.K. BINIENDA, M.J. PINDERA, *Frictionless contact of layered metal-matrix and poly er-matrix composite half planes*, Composites Science and Technology, **50**, 1, 119–128, 1994.

Received November 12, 2021; revised version January 29, 2022.
Published online March 08, 2022.